Strongly coupled piezoelectric energy harvesters: finite element modelling and experimental validation

Yang Kuang, Zheng Jun Chew, Meiling Zhu*

*Corresponding author: m.zhu@exeter.ac.uk

College of Engineering, Mathematics and Physical Sciences, University of Exeter, Exeter, EX4 4QF, UK

Abstract

Piezoelectric energy harvesters (PEHs) are usually connected to a load resistor R_L matching to the impedance of their internal capacitance C_P^T to characterise the power generation during transducer design and optimisation. For strongly-coupled PEHs operating near resonance, this simple RC matching method underestimates the power output and fails to characterise the dual power peaks but are still often used in both simulation and experiment. This study analysed the internal impedance network and the power output characteristics of PEHs. Based on the analysis, a novel and efficient finite element model (FEM) for strongly coupled PEHs was developed and applied to a pre-stressed piezoelectric stack energy harvester (PSEH). A stationary analysis was first performed to simulate the pre-stressed state of the PSEH. The FEM then analysed the internal impedance of the pre-stressed PSEH, which was used as the optimal load resistance to simulate the electric power output. The simulated internal impedance and electric power output of the PSEH were validated by the experiment with good agreement. The FEM developed precisely predicted the electric power output, including the two identical power peaks, of the strongly coupled PSEH operating near resonance and outside resonance. In contrast, the FEM with the traditional RC matching showed only one power peak and significantly underestimated the power output near resonance, although it was still valid outside resonance. The developed FEM was also able to predict the effects of the static pre-stress and coupling efficiency figure of merit on the PSEH. The coupling efficiency figure of merit was found to increase the power output.

Keywords: piezoelectric energy harvesting; electric impedance; finite element modelling; pre-stressed; strongly coupled

Nomenclature		Z_{in}	Internal impedance of a PEH (Ω)
PEH	Piezoelectric energy harvester	$\lvert Z_{in}\rvert$	Magnitude of internal impedance (Ω)
PSEH	Piezoelectric stack energy harvester	Y_{in}	Internal admittance of a PEH (S)
FEM	Finite element model	G	Conductance, the real part of Y_{in} (S)
SDOF	Single degree of freedom	B	Susceptance, the imaginary part Y_{in} (S)
ECM	Equivalent circuit model	G_{max}	The maximum conductance value (S)
K	Electromechanical coupling coefficient	ω_s	Short circuit resonance frequency (rad/s)
Q_M	Mechanical quality factor	$B(\omega_s)$	Conductance value at ω_s (S)
K^2Q_M	Coupling efficiency figure of merit	ω_1, ω_2	Frequencies at which the conductance value is $\frac{1}{2R_m}$ (rad/s)
m	Proof mass of a PEH (kg)	ω_{01}, ω_{02}	Angular frequencies with zero impedance phase and $\omega_{01} < \omega_{02}$ (rad/s)
c_d	Damping coefficient of a PEH	f_{01}, f_{02}	Frequencies with zero impedance phase and $f_{01} < f_{02}$ (Hz)
k	Stiffness of a PEH (N/m)	f_m	The frequency with the maximum impedance phase (Hz)
x	Displacement of a PEH (m)	β	Tilted angle of the inclined beams in the mechanical transformer (°)
C_P^S	Clamped capacitance of a PEH (F)	F_x	Input force to the PSEH along the x-axis (N)
C_P^T	Free capacitance of a PEH (F)	D_x	Input displacement to the PSEH along the x-axis (m)
Λ	Force factor of a PEH (N/V)	F_z	Force applied to the piezoelectric element (N)

V_P	Output voltage on a load resistance (V)	D_z	Displacement of the piezoelectric element (m)
I_P	Output current through a load resistance (A)	k_x	Stiffness of the PSEH in the x-axis (N/m)
R_L	Load resistance (Ω)	k_z	Stiffness of the PSEH in the z-axis (N/m)
R_{opt}	The optimal load resistance (Ω)	L_z	Length of the PSEH along the z-axis (mm)
A_0	Amplitude of the harmonic acceleration (m/s^2)	ΔL_z	Change of L_z due to the pre-force (μm)
ω	Angular frequency (rad/s)	L_x	Length of the PSEH along the x-axis (mm)
C_m	Capacitance in the equivalent circuit model (F)	ΔL_x	Change of L_x due to the pre-force (μm)
R_m	Resistance in the equivalent circuit model (Ω)	N	Number of active piezoelectric layers in the multilayer piezoelectric stack
L_m	Inductance in the equivalent circuit model (H)	s_{ij}^E	Elastic compliance tensor at the constant condition (m^2/N)
V_{eq}	Voltage in the equivalent circuit model (V)	ˇ	Variables corresponding to the single-layer piezoelectric element used in the FEM
F_s	The static force applied to the mechanical transformer without the piezoelectric element in the FEM, i.e. estimated static force applied to the fabricated PSEH (N)	F_0	The static force applied to the PSEH in the FEM for impedance and power simulation

1. Introduction

Piezoelectric energy harvesting has been intensively investigated in the past two decades, aiming to provide a sustainable power source for wireless electronics by converting the ambient vibrations to usable electricity [1]. It is well known that the power output of a piezoelectric energy harvester (PEH) is highly dependent on the impedance of the load. Although complicated power management circuits are required to transfer the power efficiently from the PEHs to energy storages [2], a load resistor is usually connected to characterise the generated power during the transducer design and optimisation stage. The optimal load resistance is the one yielding the maximum power consumption on the load resistor. In the simplest form, a piezoelectric energy harvester can be considered as two decoupled mechanical and electrical systems. It is usually modelled as an equivalent circuit model with a current source connected in parallel or a voltage source connected in series to the free capacitor of the piezoelectric material [3, 4]. The optimal resistance is therefore considered as the impedance of the free capacitor (referred to as RC matching) [5]. The RC matching method has satisfactory accuracy for all PEHs operating outside the resonance [6] and for weakly coupled PEHs operating near resonance [7], due to the capacitive nature of PEHs in these cases and thereby has been widely used in both modelling and experiment. However, for strongly coupled PEHs operating near resonance, the RC matching method was found to be inaccurate [8]. For instance, the power output of strongly coupled PEHs has two identical peaks near resonance [9], which cannot be observed with the RC matching method in either experiment or simulation.

To predict the electric power output of PEHs more accurately, analytical models have been developed to derive the full expression of power output, which is then analysed to identify the optimal load resistance and peak power [10]. Through analytical models, Renno *et al.* [11] and Goldschmidtboeing *et al.* [12] found that two power peaks and two optimal load resistance values may exist near the resonance of a PEH when the electromechanical coupling coefficient K is high enough or the mechanical damping is low enough. This phenomenon was also observed by Liao and Sodano [13] in both experiment and analytical modelling. They found that if the RC matching method was used, only a single power peak could be observed, which confirmed the inaccuracy of the RC matching method for strongly coupled PEHs near resonance. Analytical models can precisely predict optimal resistance and maximum power generation. They can be quite useful for design optimisation of PEHs. However, they do not provide a physical and intuitive explanation for the power characteristics of strongly-coupled PEHs. Moreover, the closed form expression of the power output may not be available when the structure of the PEH becomes complicated or nonlinear [14, 15].

Equivalent circuit models (ECMs) of PEHs based on lumped parameters have been developed and implemented in simulation tools such as SPICE. The lumped parameters can be determined by either analytical modelling [16] or finite element analysis [17]. Kong *et al.* [18] derived the internal impedance network of PEHs based on the analogy between electrical and mechanical domains. The internal impedance network was found far more complicated than the free capacitor as used in the RC matching method. They pointed out that with a resistive impedance matching, the maximum power transfer was available at frequencies with a purely resistive internal impedance, i.e. the impedance phase is zero. When the zero-phase is not available, the load resistance should still match the internal impedance magnitude to achieve a sub-optimal matching [18]. This was further investigated by Lei *et al*. [19], who showed that when the coupling efficiency figure of merit K^2Q_M (Q_M being the mechanical quality factor) was larger than 2, the internal impedance of the PEH had two zero-phase frequencies near resonance and therefore two power peaks were available. The link of power peaks to the zero-impedance-phase provides a sensible explanation to the double power peaks of strongly coupled PEHs. ECMs with lumped parameters are useful for designing the power management circuits [20, 21] after the design of a PEH is finished and thus the lumped parameters are fixed. However, it is not convenient for the design and optimisation of energy harvesters because the design parameters such as geometry and material properties are not directly reflected in the lumped parameters [22].

For energy harvester design and optimisation, commercial software packages such as ANSYS and COMSOL provides a powerful tool because of their ability to simulate complicated transducer structures [23, 24] and more importantly to couple the fields of mechanical structures, piezoelectricity and electrical circuits. This enables the development of piezoelectric-circuit coupled finite element models (FEMs), in which piezoelectric energy harvesters are connected to electrical circuits. This provides a direct link between physical design parameters and the electric power output. The first coupled piezoelectric-circuit coupled FEM was developed by Zhu *et al.* [25] in ANAYS to analyse the power output of piezoelectric cantilever connected to a load resistor, but it is for weakly coupled piezoelectric energy harvesters although there is no mention on this. Since then, similar FEMs have been developed to simulate the performance of various PEHs [26-28]. Cheng *et al.* [22] modelled the nonlinear synchronized switch harvesting on inductor as an equivalent linear electric impedance in COMSOL thus enabling the finite element modelling of PEH connected to a nonlinear circuit. For strong coupled piezoelectric energy harvester, although the internal impedance network of a PEH is far more complicated than the free capacitor of the piezoelectric material, most FEMs still use the simple RC matching method, i.e. using a load resistance to match the impedance of the capacitor, which could lead to inaccurate results for strongly coupled PEHs operating near resonance. FEMs for strongly coupled PEHs have not been reported so far. This work proposes a novel and efficient finite element modelling method for strongly-coupled PEHs connected to a load circuit. The FEM first analyses the internal impedance of the PEH across the frequency range of interest. The impedance magnitudes are then used as the value of the optimal load resistance at the corresponding frequency to simulate the power generation. Using the proposed method, the full performance of the PEH including the optimal load resistance and the maximum power output across the whole frequency range can be accurately simulated, regardless of the degree of electromechanical coupling. The method can be applied to any harmonically actuated linear PEHs or nonlinear PEHs that can be linearized around the operating point.

2. Optimal load resistance and power out characteristics of PEHs

In this section, the theories behind the optimal load resistance and power output characteristics of PEHs are revisited to provide guidance for the finite element modelling.

2.1 Internal impedance of PEHs

The majority of piezoelectric energy harvesters can be regarded as an oscillator with single-degree-of-freedom (SDOF) and working at the fundamental mode. Considering a single SDOF PEH subjected to harmonic excitation at its base, its dynamic behaviours can be described by (1) [21].

$$m\ddot{x}(t) + c_d\dot{x}\ (t) + kx(t) + \Lambda V_p(t) = mA_0cos(\omega t)$$

$$I_P(t) + C_P^S\dot{V}_P(t) = \Lambda\dot{x}(t) \qquad (1)$$

where m is the mass, c_d the mechanical damping coefficient, k the stiffness, x the displacement, C_P^S the clamped capacitance, Λ the force factor, V_P the output voltage, I_P the output current, A_0 the amplitude and ω the frequency of excitation acceleration, respectively.

According to the analogy between mechanical and electrical systems, the system described by (1) can be represented by an equivalent circuit model as shown in Figure 1 (a). The inertial mass m, compliance $1/k$ and mechanical damping c_d are represented by the inductor, capacitor, and resistor respectively. The electromechanical coupling of the piezoelectric element is represented as an ideal transformer with a transformation factor of Λ: 1. The excitation force is modelled as a harmonic voltage source with an amplitude of mA. The model in (a) can be simplified to (b) by taking the equivalence in (2).

$$C_m = \frac{\Lambda^2}{k} \qquad R_m = \frac{c_d}{\Lambda^2}$$

$$L_m = \frac{m}{\Lambda^2} \qquad V_{eq} = \frac{mA}{\Lambda} \tag{2}$$

where C_m, R_m, L_m and V_{eq} are the capacitance, resistance, inductance and equivalent voltage, respectively.

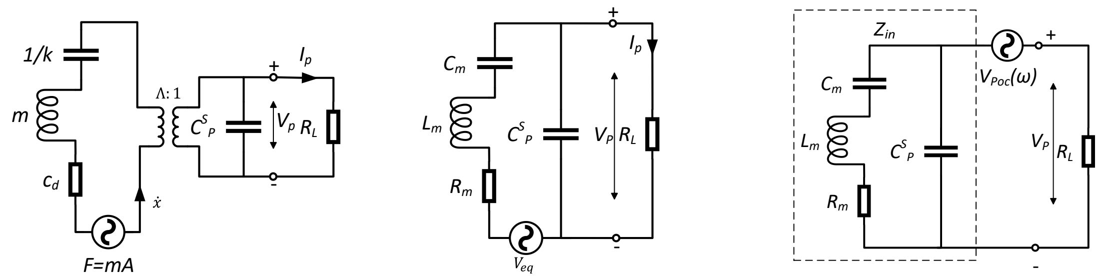

(a) (b) (c)

Figure 1 Equivalent circuit models of single-degree-of-freedom piezoelectric energy harvesters operating near the fundamental resonance: (a) original equivalent circuit model; (b) simplified model by taking the transformer equivalence; (c) resultant model by applying Thevenin's Theorem on (b)

The ECM in Figure (b) can be further transformed to Figure (c) by applying Thevenin's Theorem. In Figure (c), the PEH is modelled as an AC voltage source with an internal impedance Z_{in} connected in series to R_L. The amplitude of the voltage source is the output voltage V_P measured at open-circuited condition, denoted as $V_{Poc}(\omega)$ and is frequency-dependent. The internal impedance network consists of a motional branch (C_m, L_m and R_m) and the clamped capacitor C_P^S connected in parallel. It is clearly far more complicated than just a capacitor, which is assumed when using the RC matching method.

The values of the components in the ECMs can be identified from the measured or simulated internal impedance characteristics by using (3) [29].

$$R_m = \frac{1}{G_{max}} \qquad C_P^S = \frac{B(\omega_s)}{\omega_s}$$

$$C_m = \frac{\omega_2 - \omega_1}{R_m \omega_1 \omega_2} \qquad L_m = \frac{1}{\omega_s^2 C_m} = \frac{R_m}{\omega_2 - \omega_1} \tag{3}$$

where ω_s is the short-circuit resonance frequency that has the maximum conductance value G_{max}; $B(\omega_s)$ the susceptance value at ω_s; ω_1 and ω_2 are the two frequencies with a conductance value of $1/(2R_m)$. The voltage V_{eq} can be calculated as

$$V_{eq} = I_{sc}(\omega_s) R_m \tag{4}$$

where $I_{sc}(\omega_s)$ is the short-circuited current generated at ω_s.

2.2 Power output characteristics of PEHs with resistive impedance matching

At each frequency, the PEH is a voltage source V_{Poc} with a complex internal impedance Z_{in}. According to the maximum power transfer theorem, the maximum power delivery occurs only when the load is a complex conjugate matching of Z_{in}. The maximum power that can be delivered is [18]

$$P_{max} = \frac{V_{eq}^2}{8R_m} \tag{5}$$

However, a complex conjugate matching across the whole resonance range is difficult because of the large and varied inductance required at different frequencies [18]. Instead, a load resistor is usually used to match the internal impedance in the energy harvester design stage. With a resistive load, the conjugate impedance matching occurs when the phase of the internal impedance is zero, i.e. the internal impedance is purely resistive. In such a case, the maximum power transfer occurs and P_{max} is delivered to the load resistance. At frequencies with non-zero-phase, conjugate impedance matching is not possible with a resistive load and therefore the maximum power transfer cannot be achieved. However, the load resistance should still be selected to match $|Z_{in}|$ to obtain the sub-maximum power although this power will be lower than P_{max}. Therefore, with a resistive load, power peaks of a PEH are located at zero-phase frequencies if available and the number of power peaks depends on the number of zero-phase frequency.

When the impedance phase of the PEH is always negative, a conjugate impedance matching is not possible with the resistive load across the whole resonance region. In this case, a single power peak occurs at the frequency with the maximum internal impedance-phase because at this frequency, the internal impedance has the minimum reactive component, i.e. it is mostly close to being purely resistive, which has been mathematically proved in [19].

At low frequencies where the PEH can be regarded as quasi-static, the contribution of L_m and R_m to Z_{in} is negligible compared to C_m. As a result, the internal impedance network can be approximated by C_m and C_P^S connected in parallel, which equals to the free capacitor C_P^T of the PEH [17]. This leads to the traditional RC matching method with the optimal load resistance R_{opt} being

$$R_{opt} = \frac{1}{\omega C_P^T} \tag{6}$$

2.3 Conditions for the existence of zero-phase frequencies

Since the zero-phase frequency plays an important role in the power output characteristics of PEHs, the conditions for its existence are derived in this section by using a more intuitive method—graphic analysis than the traditional analytical modelling [19]. Instead of using the internal impedance directly, the admittance of the internal impedance network was used because the unique characteristics of conductance and susceptance can simplify the analysis. It is noted that the phase of the admittance is opposite to that of the impedance.

The complex admittance Y_{in} of the internal impedance network shown in Figure 1 (c) is [30]

$$Y_{in} = \frac{1}{Z_{in}} = \frac{R_m}{R_m^2 + \left(\omega L_m - \frac{1}{\omega C_m}\right)^2} + j\left[\omega C_P^S - \frac{\omega L_m - \frac{1}{\omega C_m}}{R_m^2 + \left(\omega L_m - \frac{1}{\omega C_m}\right)^2}\right] \tag{7}$$

The real and imaginary parts of the Y_{in} are the conductance G and susceptance B, respectively. The relationship between G and B near resonance can be re-written as

$$\left(G - \frac{1}{2R_m}\right)^2 + (B - \omega_s C_P^S)^2 = \left(\frac{1}{2R_m}\right)^2 \tag{8}$$

The typical locus of G-B for a PEH is presented in Figure 2 (a). It is a circle with a diameter of $1/R_m$ and its centre O_1 at $(1/(2R_m), \omega_s C_P^S)$. The two intersections of the G-B locus with B=0 (G-axis), denoted as $\omega_{01}$and ω_{02}, are corresponding to the zero-phase frequencies, at which a complex conjugate impedance matching by a load resistance is available. Therefore, a PEH with a G-B circle as Figure 2 (a) has two power peaks across near resonance. Obviously, ω_{01} and ω_{02} are always available as long as $\omega_s C_P^S < 1/(2R_m)$. Considering the mechanical quality factor Q_M and the electromagnetic coupling factor K in (9) [8, 17], the condition for the existence of ω_{01} and ω_{02} can be rewritten by (10), which agrees with the expression derived by using maa thematical method in [19].

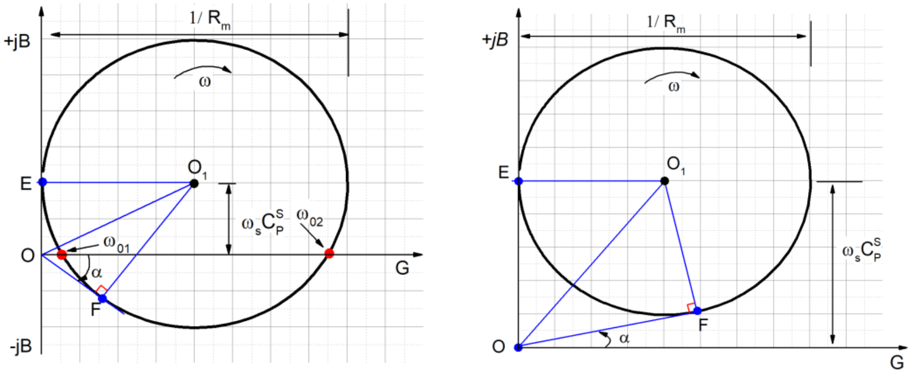

(a) (b)

Figure 2 Locus diagram of the internal admittance of a piezoelectric energy harvester near resonance when: (a) $\omega_s C_P^S < 1/(2R_m)$, i.e. $K^2 Q_M$>2 and (b) $\omega_s C_P^S > 1/(2R_m)$, i.e. $K^2 Q_M$<2. G-axis is located at B=0

$$Q_M = \frac{\omega_s}{\omega_2 - \omega_1} = \frac{1}{\omega_s R_m C_m} \qquad K^2 = \frac{\Lambda^2}{k C_P^S} = \frac{C_m}{C_P^S} \tag{9}$$

$$K^2 Q_M > 2 \tag{10}$$

When $\omega_s C_P^S > 1/(2R_m)$ or $K^2 Q_M < 2$, the G-B circle has no intersection with the B=0, i.e. no zero-phase frequency as shown in Figure 2 (b). Compared to figure (a), the centre of the G-B circle in (b) was moved-up while the diameter was kept unchanged, simulating the case when C_P^S is increased (K is reduced according to (9)). The loss of zero-phase can also be caused by the shrink in the diameter of the G-B circle due to increased mechanical damping R_m, which will be demonstrated in Section 5.4. Without the zero-phase frequency, the power peak is available at the maximum-impedance-phase frequency (the minimum-admittance-phase frequency), although conjugate impedance matching is not possible with a resistive load. When $\omega_s C_P^S = 1/(2R_m)$ or $K^2 Q_M = 2$, the G-B locus will have one intersection with $B = 0$ and a single power peak is available at the single zero-phase frequency.

It is noted that the internal admittance magnitude of the PEH at the minimum-admittance-phase frequency is always $\omega_s C_P^S$ regardless of $K^2 Q_M$. The minimum admittance-phase frequencies correspond to point F in Figure 2, where the line $\overline{OF}$ is tangent to G-B locus. The angle α between $\overline{OF}$ and G-axis is the minimum admittance phase in each case. Because triangles OO_1E and OO_1F are congruent, $|\overline{OF}|$ always equals to $|\overline{OE}|$ and $\omega_s C_P^S$. In other words, the internal impedance magnitude and the optimal load resistance of a PEH at the maximum-impedance-phase frequency is always $1/(\omega_s C_P^S)$.

In light of the importance of $K^2 Q_M$ on the power output characteristics of PEH, $K^2 Q_M$ is usually referred to as the coupling efficiency figure of merit [19]. PEHs with $K^2 Q_M$ >2 are strongly-coupled, have two zero-phase frequencies and two power peaks near resonance; PEHs with $K^2 Q_M \leq 2$ are weakly-coupled, have a single or no zero-phase frequency and a single power peak near resonance.

3. Piezoelectric stack energy harvester

A piezoelectric stack energy harvester (PSEH) with a mechanical transformer was used to study in this work, which is a good example of strongly coupled PEH. Similar harvesters have been widely studied for low-frequency compressive force energy harvesting [31-34] due to the high electrical power output, which is a result of the force amplification mechanism and the high electromechanical coupling of piezoelectric stacks used [35].

3.1 Working mechanism

A schematic of the PSEH with a mechanical transformer is shown in Figure 3. It consists of a mechanical transformer and a piezoelectric element usually in the form of a multilayer piezoelectric stack. The inclined beams of the mechanical transformer have a tilted angle β. Both ends of each inclined beam serve as flexure hinges. To simplify the analysis, it is assumed that the hinges are free to flexure while the inclined beams do not change its length. In a quasi-static state, the following relationship can be obtained [33, 36]

$$F_z = F_x \cot\beta \qquad D_x = D_z \cot\beta \tag{11}$$

where F_x and D_x are the input force and displacement; F_z and D_z are the force and displacement of the piezoelectric element.

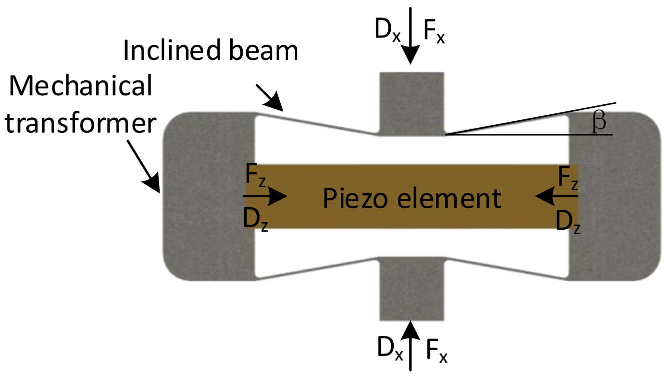

Figure 3 The operation principle of the PSEH with a mechanical transformer

Eq. (11) suggests that when β is small, the mechanical transformer amplifies the input force F_x by a factor of $\cot\beta$ to the force F_z applied on the piezoelectric element. It is this force amplification mechanism that attracts the wide interests from energy harvesting research community because the electric power output of a PEH increases proportionally with the square of the force applied on the piezoelectric material. Eq. (11) also indicates that while amplifying the force, the mechanical transformer reduces the displacement D_x by a factor of $\cot\beta$. This leads to the stiffness along x-axis (k_x) to be lower than that along z-axis (k_z) since

$$k_x = \frac{F_x}{D_x} = \frac{1}{\cot^2\beta} \cdot \frac{F_z}{D_z} = \frac{k_z}{\cot^2\beta} \tag{12}$$

Piezoelectric elements have high stiffness, leading to a resonance frequency usually in the range of tens of kilohertz, in contrast to the usual low frequencies (from a few to hundreds of hertz) of ambient vibrations. The reduction in the stiffness can lower the resonance frequency of the PSEH to match the ambient vibration. Although Eqs. (11-12) can be used for qualitative analysis, it must be noted that in reality, the relationship between the force/displacement amplification and the tilted angle is more complicated due to the elastic deformation of the inclined beams [33, 34, 36].

3.2 Design, fabrication and testing method

The PSEH designed for this study is shown in Figure 4 (a). Given that the focus of this study is the modelling of the PSEH, the design optimisation of the mechanical transformer is not presented herein. Notably, a notch hinge design was used for the inclined beams where the thickness of the flexure hinges was much smaller than the middle section of the inclined beam. This is to allow easy bending of the hinges while reducing the elastic deformation and energy storage in the inclined beams [36].

A multilayer piezoelectric stack (7×7×36 mm, PI ceramic) was used for the PSEH. The piezoelectric stack is made of ~560 layers of active piezoelectric material working at 33-mode (PIC252, layer thickness: ~60 µm including electrodes) and 2 passive piezoelectric layers (~0.5 mm thick), one on each end. The active piezoelectric layers are electrically connected in parallel. The mechanical transformer was made of spring steel and fabricated by electrical discharge machining. The space on the mechanical transformer was machined to be ~50 µm shorter than the multilayer piezoelectric stack as shown in Figure 4 (b). During assembling, the mechanical transformer was stretched along the z-axis so that the piezoelectric stack could slide into space. Upon release, the mechanical transformer was subjected to deformation, leading to an increase in both L_x (denoted as ΔL_x) and L_z (denoted as ΔL_z). As a result, the mechanical transformer applied a static compressive force to the piezoelectric stack, which is essential for reliable operation since piezoelectric material has low tensile strength and high compressive strength. Adhesive epoxy was used on the interfacing surfaces between the piezoelectric stack and the mechanical transformer to further secure the connection. After assembling, ΔL_z and ΔL_x was measured by a micrometer (resolution of 10 µm) as 69 and 660 µm, respectively.

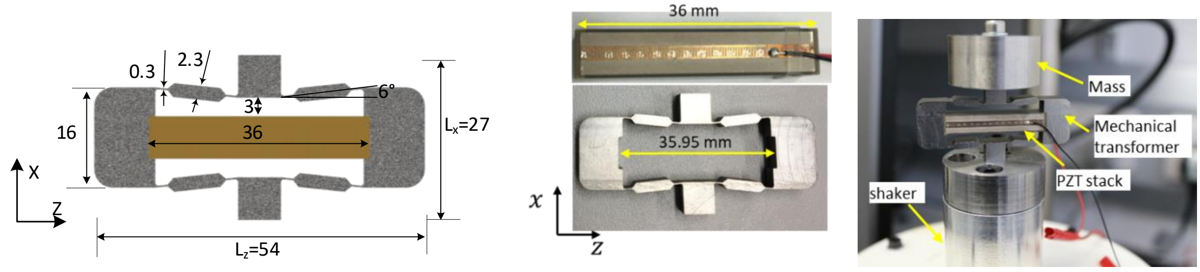

(a) (b) (c)

Figure 4 (a) Designed PSEH with a mechanical transformer: unit in mm unless specified, (b) the fabricated mechanical transformer and multilayer piezoelectric stack used for the PEH, and (c) fully assembled PSEH installed on a shaker for testing

The fabricated PSEH is shown in Figure 4 (c). A 100-gram mass was added on the PSEH to produce inertial force and reduce the resonance frequency. The internal impedance of the PSEH was measured by a frequency response analyser (PSM1700, Newton 4th). The internal impedance was converted to admittance to calculate the mechanical quality factor Q_M by using (9). To measure the electric power generation, the PSEH was installed on an electromagnetic shaker (V20, Data Physics). The harmonic acceleration produced by the shaker was measured by a laser Doppler vibrometer (CLV 2534, Polytech). The PSEH was connected to a variable load resistor, the voltage across which was recorded to calculate the power output. For each excitation frequency, the load resistor was varied until the maximum power and the optimal load resistance were found.

4. Finite element modelling methods

Finite element modelling was used to aid the design of the PSEHs [31, 34, 36]. However, these FEMs were only able to simulate the mechanical responses, not the electrical output, which severely limits their usefulness. Moreover, the PSEHs are usually strongly coupled but the RC matching method was used in modelling and may lead to inaccurate results. Furthermore, static compressive stress on the piezoelectric stacks is essential to compensate for their weakness to tensile stress. The static prestress may affect the performance of the PSEH but the effects have not been modelled.

A finite element model of the PSEH described in Section 3.2 was therefore developed in COMSOL Multiphysics ® (COMSOL Inc, UK), which is able to accurately predict the power output of the pre-stressed and strongly coupled energy harvester. Because the analysis in Section 2 suggests that the optimal load resistance is the internal impedance magnitude, the internal impedance is first simulated in the developed FEM and is then used as the load resistance for power generation simulation. The method described in this section can be used for any harmonically excited linear PEHs or nonlinear PEHs that can be linearized around the operating point. The PEHs can be connected to a linear interfacing circuit that does not contain nonlinear components such as diodes and transistors.

4.1 General considerations

The 3D physical model is comprised of the mechanical transformer and the piezoelectric element, which is shown in Figure 5 in 2D for better presentation. The dimensions are shown in Figure 4 (a). A 100-gram mass was added to the top surface of the mechanical transformer by applying COMSOL boundary condition without building a physical mass. The dimension of the piezoelectric element was 7×7×36 mm, which was all treated as active material in the model since the volume fraction of the passive layer was only 2.7% of the multilayer piezoelectric stack. The mechanical damping of the PSEH was specified as a mechanical quality factor Q_M.

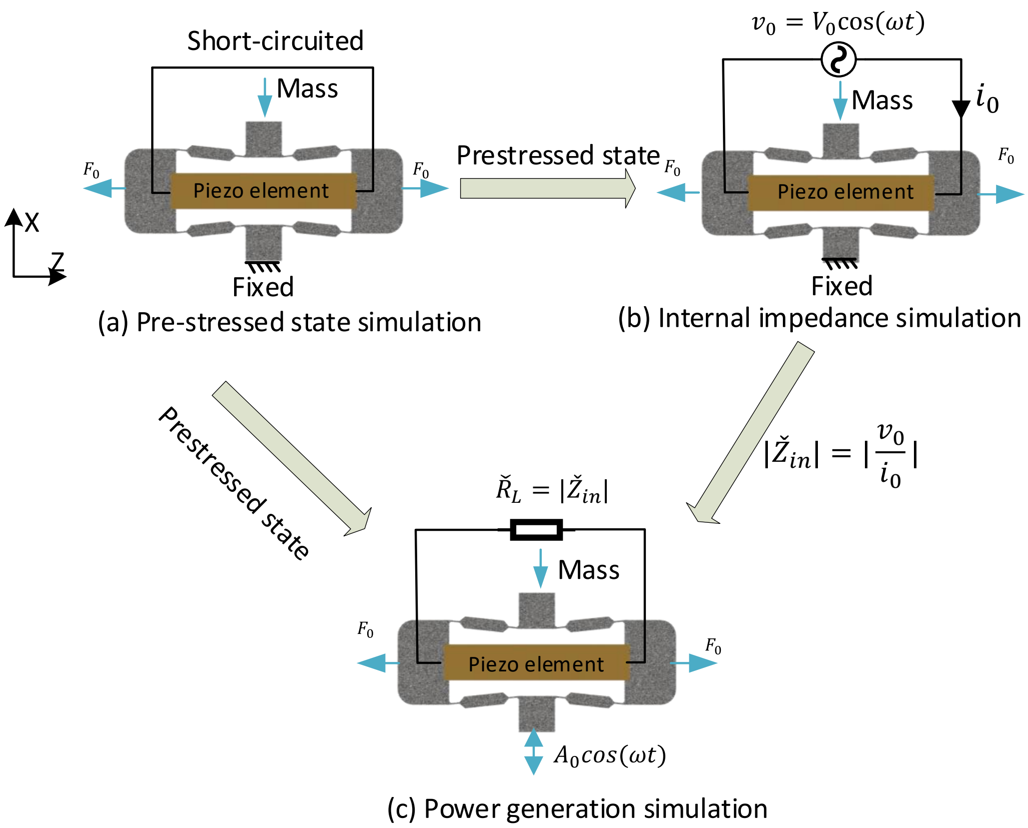

Figure 5 3D model and boundary conditions of the PSEH in (a) pre-stressed state simulation (b) internal impedance simulation and (c) power generation simulation

The multilayer piezoelectric stack was modelled as a single-layer piezoelectric element with the same overall dimensions and polarised along the z-axis to simplify the model and reduce the computational time. The number of layers does not affect power output and resonance frequencies but affects some values such as impedance magnitude and voltage. To facilitate the comparison between simulation and experiment, the values of the single-layer stack were converted to the equivalent values of a multilayer stack by (13).

$$\Gamma = \frac{\check{\Gamma}_s}{N^2} \quad C = N^2\check{C} \quad V_P = \frac{\check{V}_P}{N} \tag{13}$$

Γ stands for the impedance magnitude $|Z_{in}|$, load resistance R_L, inductance L_m; C stands for capacitance C_P^S, C_P^T and C_m; N=560 is the number of layers; V_P is the voltage output. The symbols with an accent ˇ denote the values for the single-layer piezoelectric element, while those without an accent denote the converted values for multilayer piezoelectric stack. The material properties used for simulation are presented in Table 1. As the multilayer piezoelectric stack includes not just piezoelectric material (PIC252) but also electrodes, its elastic compliance is different from the piezoelectric material. The elastic compliance along z-axis is particularly important because the piezoelectric stack vibrates along this direction. The elastic compliance of the piezoelectric stack s_{33}^E was estimated based on the stiffness (50 N/μm)) of the multilayer stack provided by the supplier, instead of using the material properties of PIC252.

Table 1 the material properties of the multilayer piezoelectric stack and spring steel

Parameters	Values
Piezoelectric stack	
Density (kg/m^3)	7800
s_{11}^E (×10^{-12} m^2/N)	16.06
s_{12}^E(×10^{-12} m^2/N)	-5.68
s_{13}^E(×10^{-12} m^2/N)	-7.45
s_{33}^E(×10^{-12} m^2/N)	27.0
s_{44}^E(×10^{-12} m^2/N)	46.99
s_{66}^E(×10^{-12} m^2/N)	43.50
d_{31}(×10^{-12} m/V)	-186.7
d_{33} (×10^{-12} m/V)	399.6
d_{15} (×10^{-12} m/V)	617.4
$\varepsilon_{11}^T/\varepsilon_0$	1852
$\varepsilon_{33}^T/\varepsilon_0$	1751
Spring steel	
Density (kg/m^3)	7850
Young's modulus (GPa)	207
Poisson's ratio	0.3

In the fabricated PSEH, the mechanical transformer was stretched to apply to static compressive stress on the piezoelectric element. As a result, a static tensile force was applied to the mechanical transformer, leading to a reduced inclined angle β. The reduction β is expected to reduce the stiffness and resonance frequency of the PSEH, as analysed in Section 3.1. To simulate this effect, a static force F_0 was applied to the PSEH as shown in Figure 5. The static force stretched the mechanical transformer and reduced β, which is the same as the case of the fabricated PSEH. The static force in the FEM also introduced static tensile stress in the piezoelectric element, which is opposite to the case of the fabricated PSEH. This does not affect the validity of the modelling because the static stress in the piezoelectric element does not affect the power output. The magnitude of F_0 in the FEM was set to a value that produced the same ΔL_z as in experiment (66 μm).

4.2 Boundary conditions

The developed FEM consists of three analysis steps incorporated in one study. Step (1), pre-stressed state simulation, is a stationary analysis which computes the pre-stressed state of the PSEH as a result of the static force. The pre-stressed state obtained in this step is passed to the next two steps. Step (2) and (3) are 'frequency domain, perturbation analysis', which computes the response of the PSEH subjected to a harmonic perturbation fluctuating around the pre-stressed state computed in Step (1). Step (2) simulates the internal impedance of the pre-stressed PSEH, which is passed to Step (3) for power generation simulation. The relationship between the three steps is shown in Figure 5. The boundary conditions for each step are described below. For PEHs without pre-stress, Step (1) can be omitted.

(1) Pre-stressed state simulation

In this step, the piezoelectric element was short-circuited and a static force was applied to simulate the mechanical responses without electromechanical coupling, as shown in Figure 5 (a). The bottom surface of the mechanical transformer was fixed to make sure that enough degrees of freedom were constrained in the simulation.

(2) Internal impedance simulation

In this step, the bottom of the mechanical transformer was fixed as step (1). A harmonic voltage v_0 was applied to the electrodes of the piezoelectric element, as shown in Figure 5 (b). A frequency sweep across the frequency range of interest was performed. The current i_0 simulated was used to compute the internal impedance of the PSEH at each frequency by

$$\check{Z}_{in} = \frac{v_0}{i_0} = |\check{Z}_{in}|e^{-j\theta_{in}} \tag{14}$$

where θ_{in} is the internal impedance phase.

(3) Power generation simulation

In this step, a harmonic acceleration was applied to the bottom of the mechanical transformer as shown in Figure 5 (c). The electrodes of the piezoelectric element were connected to a circuit with a load resistor $\check{R}_L$. $\check{R}_L$ was set to the internal impedance magnitude $|\check{Z}_{in}|$ computed in Step (2), by using the built-in operator 'withsol' provided by COMSOL. In this way, during a frequency sweep, $\check{R}_L$ was always equal to $|\check{Z}_{in}|$ at the frequency that is being swept. The voltage across $\check{R}_L$ was recorded to compute the electric power output. For the purpose of comparison, a simulation was also performed by using the RC matching method, where $\check{R}_L$ was set to $1/\omega\check{C}_P^T$.

4.3 Estimation of the static force in the fabricated PSEH

F_0 used for internal impedance and power generation simulations is much higher than the static force in the fabricated PSEH. This is because in these simulations both the mechanical transformer and the piezoelectric were stretched by F_0 to produce ΔL_z=66 whereas in the fabricated PSEH only the mechanical transformer was stretched to produce ΔL_z = 66 µm. To estimate the static force in the fabricated PSEH, a stationary analysis was performed on the mechanical transformer without the piezoelectric element, as schematically shown in Figure 6. The mechanical transformer was stretched by a static force F_s along z-axis to reach a displacement of ΔL_z= 66 µm. This F_s was the static force applied in the fabricated PSEH.

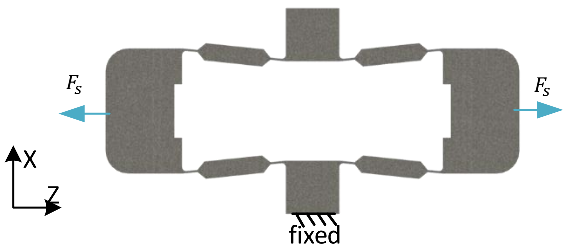

Figure 6 A schematic of the finite element model to estimate the static force F_s applied in the fabricated PSEH

5. Results and discussions

5.1 Experimental validation of internal impedance simulation

The simulated and measured internal impedance magnitudes are compared in Figure 7. In the simulation, the mechanical quality factor Q_M was set to 60, which was obtained from the measured internal impedance characteristics and by using (9). The static F_0 was initially set to produce ΔL_z=66 µm, which is the deformation measured on the fabricated PSEH. However, with ΔL_z=66 µm the simulated resonance frequency was higher than the experiment. F_0 was then adjusted until the simulated resonance frequency matched the experiment. When ΔL_z =76 µm was produced, good agreement between the measured and simulated impedance was observed. Based on the simulated internal impedance, the parameters of the equivalent circuit model were identified by using (3) and listed in Table 2. The effective electromechanical coupling factor K was calculated by (9). Considering Q_M is 60, the value of K^2Q_M is 7.8, which is larger than 2. Therefore, the PSEH modelled in this work is strongly coupled.

Both simulated and measured internal impedance have zero-phase at 189 and 200.5 Hz. The maximum-phase is observed at 195 Hz. At this frequency, impedance magnitude is 159 **Ω**, which is close to the value of $1/(\omega_s C_P^S)$=156 **Ω**. This agrees with the theoretical analysis in Section 2 that the internal impedance magnitude at the maximum-phase frequency is $1/(\omega_s C_P^S)$.

The difference in ΔL_z between simulation and experiment is attributed to (1) the geometrical difference between the designed and fabricated mechanical transformer due to manufacturing tolerance; (2) the properties of the piezoelectric material typically varies ±5-10% compared to the datasheet.

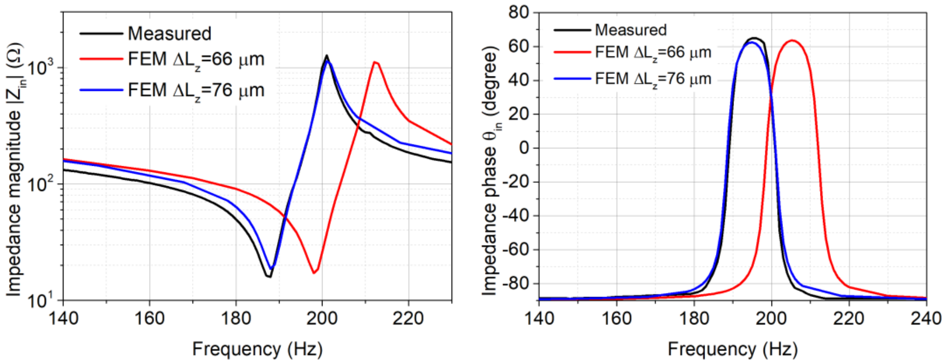

(a) (b)

Figure 7 Comparison of measured and simulated internal impedance of the PSEH (a) impedance magnitude and (b) impedance phase

Table 2 Lumped parameters identified from the simulated internal impedance of the PSEH

Parameters	Values	Unit
C_P^S	5.40	µF
C_m	0.71	µF
C_P^T	6.11	µF
ω_s	1190 (189)	Rad/s (Hz)
L_m	1.00	H
R_m	19.93	Ω
K	0.36	-

5.2 Estimation of the static force in the fabricated PSEH

When ΔL_z=76 µm was produced in the FEM (Figure 8 (a)), the static force F_0 was 4100 N. The corresponding ΔL_x was found to be 770 µm, as shown in Figure 8 (b). The displacement ratio of the PSEH, $\Delta L_x/\Delta L_z$ in the FEM is 10.13, which is close to the value of 9.50 in the experiment. Without the piezoelectric element, F_s=360 N was required to produce ΔL_z = 76 µm as shown in Figure 9 (a). Therefore, the static force applied in the fabricated PSEH is estimated to be 360 N. With F_s=360 N, ΔL_x of the mechanical transformer alone is 807 µm (Figure 9 (b)), which is slightly higher than that of the simulated PSEH. The slight difference in ΔL_x reflects the influence of the piezoelectric element on the amplification effect of the mechanical transformer.

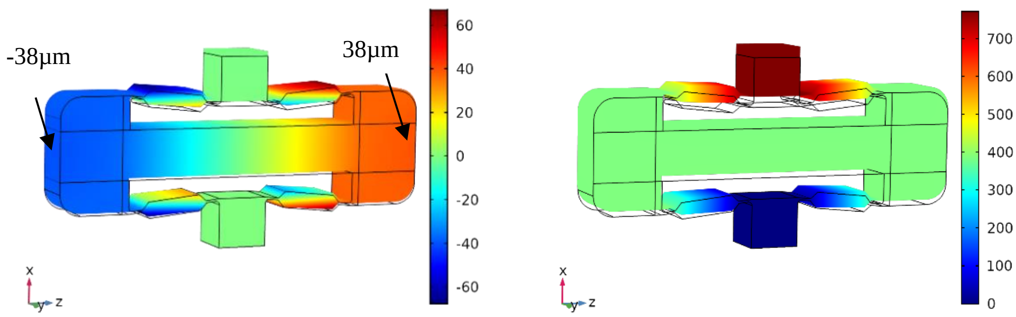

(a) (b)

Figure 8 Displacement of the PSEH due to the static force F_0=4100 N (a) z-axis displacement and (b) x-axis displacement. Unit of the colour legend: µm

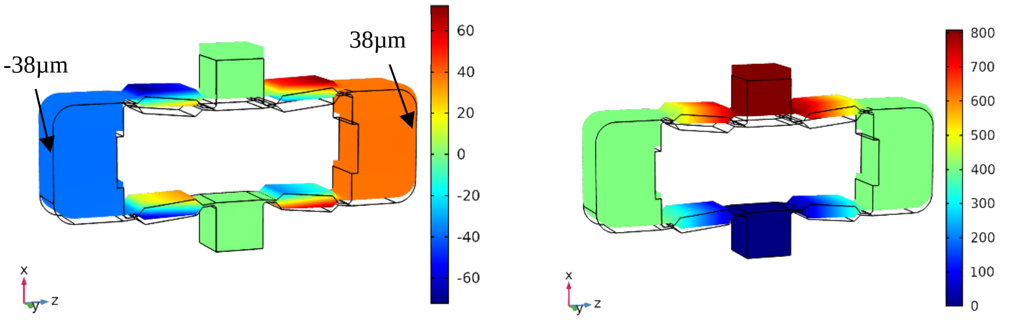

(a) (b)

Figure 9 Displacement of the mechanical transformer due to F_s=360 N: (a) z-axis displacement and (b) x-axis displacement. Unit of the colour legend: μm

5.3 Experimental validation of power generation simulation

The measured and simulated electric power outputs of the PSEH actuated at 2.5 m/s^2 are compared in Figure 10 (a). The corresponding load resistance used for the power generation is presented in Figure 10 (b). When the internal impedance magnitude $|Z_{in}|$ is used as the load resistance, the simulated electric power shows two nearly identical peaks of 5.19 and 5.22 mW at 189 and 200.5 Hz, respectively. Both frequencies are the zero-phase frequency, as identified in Section 5.1. The impedance magnitudes at these two frequencies are 19.9 and 1130.2 Ω, respectively. Moreover, the simulated power shows a local minimum of 4.21 mW at 195 Hz, which is the maximum-phase frequency. Simulations were performed at each frequency with various load resistance to confirm that the power output with $R_L = |Z_{in}|$ is the maximum at each frequency and the impedance magnitudes are the optimal load resistance. Representative results are presented in Figure 11. When actuated at 189 Hz, the PSEH produces the maximum power of 5.19 mW at 19.5 Ω.

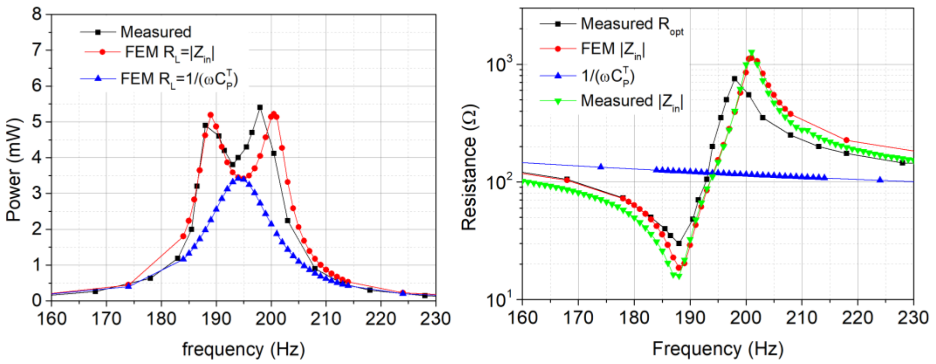

(a) (b)

Figure 10 Comparison of the measured and simulated performance of the PSEH actuated at 2.5 m/s^2 (a) electric power output (b) load resistance and internal impedance magnitude

In the experiment, the power output (Figure 10 (a)) shows two peaks of 4.90 mW and 5.4 mW at 188 and 198 Hz, respectively. A local minimum of 3.8 mW was recorded at 193 Hz. The optimal resistance at each frequency was measured by varying the connected load resistance until the maximum power output was recorded. Typical results are shown in Figure 11. The PSEH at 188 Hz produced 4.90 mW with R_L=35 Ω. The experiment results in Figure 10 show good agreement with the simulation although slight discrepancy is observed. Moreover, the measured power peaks are located at 188 and 198 Hz, instead of the zero-phase frequencies (189 and 200.5 Hz) identified in the measured internal impedance. This is caused by the nonlinear behaviours of piezoelectric material in the experiment, which was not modelled in the simulation. When piezoelectric materials are actuated to operate at high stress/strain level, the material properties will change and the behaviours become nonlinear, leading to phenomena such as reduced resonance frequency and increased mechanical loss [19, 37]. These nonlinear behaviours also caused the difference between the measured optimal resistance R_{opt} and the measured impedance magnitude since the impedance was measured at a low voltage level (0.5 V peak to peak) with little nonlinear behaviour.

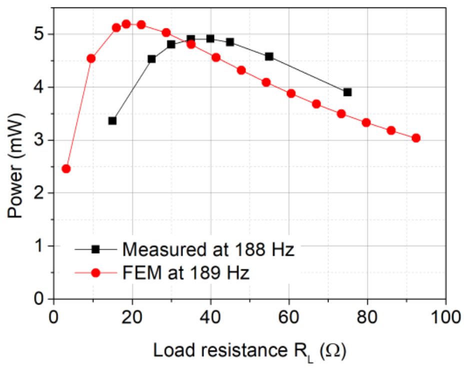

Figure 11 Electric power outputs against load resistance at the first power-peak frequency

When the RC matching method is used, i.e. $R_L = 1/(\omega C_P^T)$, the simulated power shows only one peak of 3.42 mW at 195 Hz, in contrast to two power peaks of 5.2 mW when $R_L = |Z_{in}|$. Both simulation configurations produce the same power output at the maximum-phase frequency (195 Hz). This is because the value of $1/(\omega C_P^T)$ at 195 Hz is 134 Ω, which is close to the impedance magnitude $1/(\omega_s C_P^T)$ at this frequency. This can be verified by the intersection of $|Z_{in}|$ and $R_L = 1/(\omega C_P^T)$ at around 195 Hz, as shown in Figure 10 (b). Moreover, at frequencies outside the resonance (>205 Hz and <175 Hz), the same power outputs are observed with the two simulation configurations due to the relatively small difference between $|Z_{in}|$and $1/(\omega C_P^T)$. At other frequencies, the simulation with $R_L = 1/(\omega C_P^T)$ underestimates the power output.

Therefore, with the $|Z_{in}|$ as the optimal load resistance, the FEM can accurately predict the power output of the PSEH in both resonance and off-resonance regions, whereas the FEM with RC matching can only predict the power output at the maximum-phase frequency and at off-resonance.

5.4 Effects of K^2Q_M

The theoretical analysis in Section 2 indicates that the coupling efficiency figure of merit K^2Q_M determines if there exist two power peaks of a PEH. When $K^2Q_M > 2$, the PEH is strongly coupled and has two power peaks; when $K^2Q_M \leq 2$, the PEH is weakly coupled and has a single power peak. To verify the ability of the FEM to predict such characteristics, simulations were performed on the PSEH with K^2Q_M of 7.8, 3.9, 2 and 1.3. This was achieved by keeping the effective electromechanical factor K constant at 0.36 while changing the mechanical quality factor Q_M to be 60, 30, 15 and 10, respectively. The simulated electric power outputs of the PSEH actuated at 2.5 m/s^2 along with the impedance-phase are presented in Figure 12.

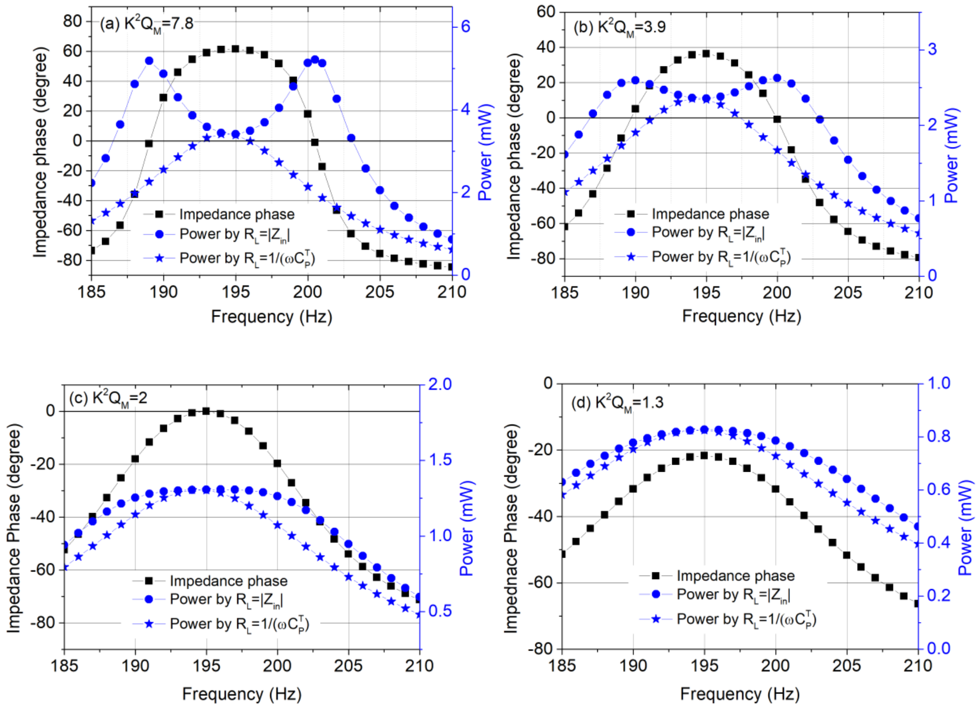

Figure 12 Simulated electric power output and impedance-phase of the PSEH with different values of K^2Q_M (a) $K^2Q_M=7.8$, (b) $K^2Q_M=3.9$, (c) $K^2Q_M=2$, and (d) K^2Q_M=1.3

When K^2Q_M=7.8 and $R_L=|Z_{in}|$, the power peaks appear at f_{01}= 189 Hz and f_{02}=200.5 Hz. The local minimum power is located at the maximum-phase frequency (f_m=195 Hz). The frequency range between f_{10} and f_{02} is 11.5 Hz. With $R_L=1/\omega C_P^T$, the single peak power is located at f_m=195 Hz. When the K^2Q_M is reduced to 3.9 (Figure 12 (b)), the PSEH has similar power-frequency characteristics as $K^2Q_M=7.8$ but with power peaks reduced from 5.22 mW to 2.62 mW and the frequency range between f_{01} and f_{02} decreased from 11.5 Hz to 10 Hz. The reduction in the power output is due to the increased mechanical damping by decreasing Q_M. Because of the decrease in Q_M, the value of R_m is increased according to Eq. (9). This leads to a decrease in the diameter of the G-B circle, as shown in Figure 13. As a result, the frequency range between f_{01} and f_{02} is decreased. When K^2Q_M is 2, the G-B cicle is tangent to B=0. As a result, f_{01}, f_{02} and f_m merges to one frequency—195 Hz and the PSEH has a single power peak at this frequency (Figure 12 (c)). As the value of K^2Q_M is further decreased, the PSEH has no zero--phases and a sinlge power peak is observed at the maximum-phase-frequency. The performance of the PSEH simulated by the FEM, therefore, agrees well with the theoretical prediction in Section 2.2.

It can be also noted from Figure 12 that as K^2Q_M is reduced, the descrepancy of power output between $R_L=|Z_{in}|$ and RC matching is decreased. This suggests that when K^2Q_M is low enough, the RC matching can be a valid approximation for the PSEH at the resonance region.

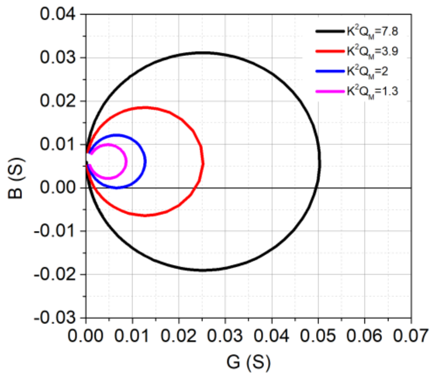

Figure 13 G-B locus of the PSEH with different values of K^2Q_M

5.5 Effects of static force

The simulated effects of the F_0 on the power output of the PSEH is presented in Figure 14. As F_0 increases, the resonance frequency decreases and the peak power increases. This is because as F_0 increases, the angle β of the mechanical transformer is reduced, which can be verified by the increase of $\Delta L_x/\Delta L_z$ with F_0 in Table 3 . As a result, the stiffness of the mechanical transformer is decreased, leading to the decrease of the resonance frequency. Moreover, the reduction of β results in an increased force amplification effect as suggested by (11), giving rise to the increase in the power generation.

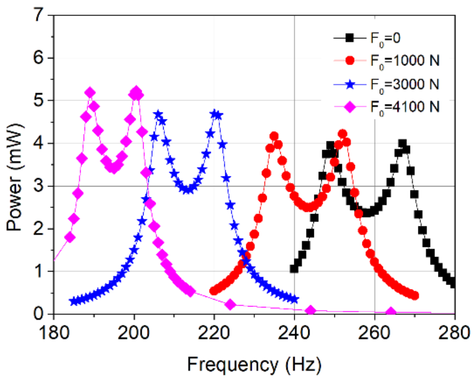

Figure 14 Effects of the static force F_0 on the power output and resonance frequency shift of the PSEH

Table 3 the static displacement ΔL_z, ΔL_x, displacement ratio $\Delta L_z/\Delta L_z$and static force F_s corresponding to each value of F_0

F_0 (N)	ΔL_z (μm)	ΔL_x (μm)	$\Delta L_x/\Delta L_z$	F_s (N)
1000	19	175	9.2	60
3000	57	554	9.8	230
4100	76	770	10.1	360

6. Conclusions

In this work, a finite element model (FEM) for strongly-coupled and pre-stressed piezoelectric energy harvester (PEH) was developed and experimentally validated. The FEM enables the efficient and accurate prediction of the electric power output of both weakly and strongly coupled PEHs. The model was developed for a piezoelectric stack energy harvester (PSEH) with a force amplifier, but the method can be applied to any linear PEHs or nonlinear PEHs that can be linearized around the operating point.

The equivalent circuit model (ECM) of PEHs was first derived from an analytical model. Based on the ECM, the internal impedance network of PEHs was identified. According to the maximum power transfer theorem, the load resistance should be matched to the internal impedance magnitude of PEHs to obtain the maximum power generation although the theoretical maximum power transfer only occurs when the impedance-phase is zero. Analysis of the conductance and susceptance locus of the internal admittance suggested that the availability of zero-phase frequency depended on the value of K^2Q_M, with K being the electromechanical coupling factor and Q_M being the mechanical quality factor.

Since the internal impedance magnitude should be used as the optimal load resistance, the proposed finite element modelling method first analysed the internal impedance of the PEH, the magnitude of which was then used as the load resistance for power output simulation. The modelling method was applied to a pre-stressed piezoelectric stack energy harvester (PSEH) with a mechanical transformer. Comparisons between simulation and experiment showed that the developed FEM was able to precisely predict both the internal impedance and electric power output of the strongly coupled PSEH at any frequencies. The simulated power output characteristics of the PSEH at different values of K^2Q_M also agreed well with the theoretical prediction. When the impedance of the internal capacitor of the PSEH was used as the optimal load resistance (RC matching), the FEM was valid at off-resonance and the maximum-phase frequency regardless of the degree of the electromechanical coupling. At resonance, the FEM with RC matching underestimated the power output for the strongly-coupled PSEH, although the error decreases with the value of $K^2 Q_M$.

Acknowledgement

The authors would like to acknowledge the finical support from the Engineering and Physical Sciences Research Council of UK (EP/S024840/1).

References

[1] A. Toprak and O. Tigli, "Piezoelectric energy harvesting: State-of-the-art and challenges," (in English), *Applied Physics Reviews,* Review vol. 1, no. 3, Sep 2014, Art no. 031104, doi: 10.1063/1.4896166.

[2] Y. Kuang, T. Ruan, Z. J. Chew, and M. Zhu, "Energy harvesting during human walking to power a wireless sensor node," *Sensors and Actuators A: Physical,* vol. 254, pp. 69-77, 2/1/ 2017, doi: http://dx.doi.org/10.1016/j.sna.2016.11.035.

[3] H. Li, C. Tian, and Z. D. Deng, "Energy harvesting from low frequency applications using piezoelectric materials," *Applied Physics Reviews,* vol. 1, no. 4, p. 041301, 2014.

[4] S. Priya, "Advances in energy harvesting using low profile piezoelectric transducers," (in English), *Journal of Electroceramics,* Article vol. 19, no. 1, pp. 167-184, Sep 2007, doi: 10.1007/s10832-007-9043-4.

[5] N. G. Elvin, A. A. Elvin, and M. Spector, "A self-powered mechanical strain energy sensor," *Smart Materials and structures,* vol. 10, no. 2, p. 293, 2001.

[6] T.-B. Xu *et al.*, "Energy harvesting using a PZT ceramic multilayer stack," *Smart Materials and Structures,* vol. 22, no. 6, p. 065015, 2013.

[7] A. Erturk and D. J. Inman, "An experimentally validated bimorph cantilever model for piezoelectric energy harvesting from base excitations," *Smart materials and structures,* vol. 18, no. 2, p. 025009, 2009.

[8] Y. Shu and I. Lien, "Analysis of power output for piezoelectric energy harvesting systems," *Smart materials and structures,* vol. 15, no. 6, p. 1499, 2006.

[9] Y. Liao and H. A. Sodano, "Structural effects and energy conversion efficiency of power harvesting," *Journal of Intelligent Material Systems and Structures,* vol. 20, no. 5, pp. 505-514, 2009.

[10] W. Wang, J. Cao, C. R. Bowen, S. Zhou, and J. Lin, "Optimum resistance analysis and experimental verification of nonlinear piezoelectric energy harvesting from human motions," *Energy,* vol. 118, pp. 221-230, 2017.

[11] J. M. Renno, M. F. Daqaq, and D. J. Inman, "On the optimal energy harvesting from a vibration source," *Journal of sound and vibration,* vol. 320, no. 1-2, pp. 386-405, 2009.

[12] F. Goldschmidtboeing, M. Wischke, C. Eichhorn, and P. Woias, "Parameter identification for resonant piezoelectric energy harvesters in the low-and high-coupling regimes," *Journal of Micromechanics and Microengineering,* vol. 21, no. 4, p. 045006, 2011.

[13] Y. Liao and H. A. Sodano, "Model of a single mode energy harvester and properties for optimal power generation," *Smart Materials and Structures,* vol. 17, no. 6, p. 065026, 2008.

[14] N. G. Elvin and A. A. Elvin, "A coupled finite element—circuit simulation model for analyzing piezoelectric energy generators," *Journal of Intelligent Material Systems and Structures,* vol. 20, no. 5, pp. 587-595, 2009.

[15] H. Abdelmoula, N. Sharpes, A. Abdelkefi, H. Lee, and S. Priya, "Low-frequency Zigzag energy harvesters operating in torsion-dominant mode," *Applied Energy,* vol. 204, pp. 413-419, 2017.

[16] N. G. Elvin and A. A. Elvin, "A general equivalent circuit model for piezoelectric generators," *Journal of Intelligent Material Systems and Structures,* vol. 20, no. 1, pp. 3-9, 2009.

[17] Y. Yang and L. Tang, "Equivalent circuit modeling of piezoelectric energy harvesters," *Journal of intelligent material systems and structures,* vol. 20, no. 18, pp. 2223-2235, 2009.

[18] N. Kong, D. S. Ha, A. Erturk, and D. J. Inman, "Resistive Impedance Matching Circuit for Piezoelectric Energy Harvesting," (in English), *Journal of Intelligent Material Systems and Structures*, Article; Proceedings Paper vol. 21, no. 13, pp. 1293-1302, Sep 2010, doi: 10.1177/1045389x09357971.

[19] A. Lei, R. Xu, L. M. Borregaard, M. Guizzetti, O. Hansen, and E. V. Thomsen, "Impedance based characterization of a high-coupled screen printed PZT thick film unimorph energy harvester," *Journal of Microelectromechanical Systems*, vol. 23, no. 4, pp. 842-854, 2014.

[20] Y. Qi, N. T. Jafferis, K. Lyons, C. M. Lee, H. Ahmad, and M. C. McAlpine, "Piezoelectric Ribbons Printed onto Rubber for Flexible Energy Conversion," (in English), *Nano Letters*, Article vol. 10, no. 2, pp. 524-528, Feb 2010, doi: 10.1021/nl903377u.

[21] J. Liang and W.-H. Liao, "Impedance modeling and analysis for piezoelectric energy harvesting systems," *IEEE/ASME Transactions on Mechatronics*, vol. 17, no. 6, pp. 1145-1157, 2012.

[22] C. Cheng, Z. Chen, H. Shi, Z. Liu, and Y. Xiong, "System-Level Coupled Modeling of Piezoelectric Vibration Energy Harvesting Systems by Joint Finite Element and Circuit Analysis," *Shock and Vibration*, vol. 2016, 2016.

[23] D. Pan and F. Dai, "Design and analysis of a broadband vibratory energy harvester using bi-stable piezoelectric composite laminate," *Energy conversion and management*, vol. 169, pp. 149-160, 2018.

[24] D. Wang, J. Mo, X. Wang, H. Ouyang, and Z. Zhou, "Experimental and numerical investigations of the piezoelectric energy harvesting via friction-induced vibration," *Energy conversion and management*, vol. 171, pp. 1134-1149, 2018.

[25] M. Zhu, E. Worthington, and J. Njuguna, "Analyses of power output of piezoelectric energy-harvesting devices directly connected to a load resistor using a coupled piezoelectric-circuit finite element method," *Ultrasonics, Ferroelectrics and Frequency Control, IEEE Transactions on*, vol. 56, no. 7, pp. 1309-1317, 2009.

[26] X. Li, D. Upadrashta, K. Yu, and Y. Yang, "Sandwich piezoelectric energy harvester: Analytical modeling and experimental validation," *Energy conversion and management*, vol. 176, pp. 69-85, 2018.

[27] K. Yang, D. Alice, and Z. Meiling, "A sandwiched piezoelectric transducer with flex end-caps for energy harvesting in large force environments," *Journal of Physics D: Applied Physics*, vol. 50, no. 34, p. 345501, 2017. [Online]. Available: http://stacks.iop.org/0022-3727/50/i=34/a=345501.

[28] Y. Kuang and M. Zhu, "Design study of a mechanically plucked piezoelectric energy harvester using validated finite element modelling," *Sensors and Actuators A: Physical*, vol. 263, pp. 510-520, 2017/08/15/ 2017, doi: http://dx.doi.org/10.1016/j.sna.2017.07.009.

[29] A. Ramos-Fernandez, J. Gallego-Juarez, and F. Montoya-Vitini, "Automatic system for dynamic control of resonance in high power and high Q ultrasonic transducers," *Ultrasonics*, vol. 23, no. 4, pp. 151-156, 1985.

[30] Y. Kuang, Y. Jin, S. Cochran, and Z. Huang, "Resonance tracking and vibration stablilization for high power ultrasonic transducers," *Ultrasonics*, vol. 54, no. 1, pp. 187-194, 2014.

[31] F. Qian, T.-B. Xu, and L. Zuo, "Design, optimization, modeling and testing of a piezoelectric footwear energy harvester," *Energy conversion and management*, vol. 171, pp. 1352-1364, 2018.

[32] X. Wang, Z. Shi, J. Wang, and H. Xiang, "A stack-based flex-compressive piezoelectric energy harvesting cell for large quasi-static loads," *Smart Materials and Structures*, vol. 25, no. 5, p. 055005, 2016.

[33] W. Chen, Y. Wang, and W. Deng, "Deformable force amplification frame promoting piezoelectric stack energy harvesting: Parametric model, experiments and energy analysis," *Journal of Intelligent Material Systems and Structures*, vol. 28, no. 7, pp. 827-836, 2017.

[34] M. Evans, L. Tang, and K. C. Aw, "Modelling and optimisation of a force amplification energy harvester," *Journal of Intelligent Material Systems and Structures*, p. 1045389X18754352, 2018.

[35] J. Cho, R. Richards, D. Bahr, C. Richards, and M. Anderson, "Efficiency of energy conversion by piezoelectrics," *Applied physics letters*, vol. 89, no. 10, pp. 104107-104107-3, 2006.

[36] L. Wang, S. Chen, W. Zhou, T.-B. Xu, and L. Zuo, "Piezoelectric vibration energy harvester with two-stage force amplification," *Journal of Intelligent Material Systems and Structures*, vol. 28, no. 9, pp. 1175-1187, 2017.

[37] Y. Kuang, M. Sadiq, S. Cochran, and Z. Huang, "High-power characterization of a microcutter actuated by PMN-PT piezocrystals," *IEEE transactions on ultrasonics, ferroelectrics, and frequency control*, vol. 62, no. 11, pp. 1957-1967, 2015.